Frontiers of Physics
https://doi.org/10.1007/s11467-020-1011-3
Front. Phys.
16(2), 22501 (2021)

RESEARCH ARTICLE

Quantum droplets in two-dimensional optical lattices

Yi-Yin Zheng*, Shan-Tong Chen*, Zhi-Peng Huang, Shi-Xuan Dai, Bin Liu, Yong-Yao Li†, Shu-Rong Wang

School of Physics and Optoelectronic Engineering, Foshan University, Foshan 528000, China
Corresponding author. E-mail: †yongyaoli@gmail.com
Received July 19, 2020; accepted September 22, 2020

We study the stability of zero-vorticity and vortex lattice quantum droplets (LQDs), which are described by a two-dimensional (2D) Gross–Pitaevskii (GP) equation with a periodic potential and Lee–Huang–Yang (LHY) term. The LQDs are divided in two types: onsite-centered and offsite-centered LQDs, the centers of which are located at the minimum and the maximum of the potential, respectively. The stability areas of these two types of LQDs with different number of sites for zero-vorticity and vorticity with $S = 1$ are given. We found that the μ–N relationship of the stable LQDs with a fixed number of sites can violate the Vakhitov–Kolokolov (VK) criterion, which is a necessary stability condition for nonlinear modes with an attractive interaction. Moreover, the μ–N relationship shows that two types of vortex LQDs with the same number of sites are degenerated, while the zero-vorticity LQDs are not degenerated. It is worth mentioning that the offsite-centered LQDs with zero-vorticity and vortex LQDs with $S = 1$ are heterogeneous.

Keywords lattice quantum droplets, optical lattices, vortex

1 Introduction

In Bose–Einstein condensates (BECs), it is well known that free-space nonlinear modes may collapse in two-dimensional (2D) and three-dimensional (3D) geometries via the action of the usual attractive cubic nonlinearity [1]. Hence, how to acquire stabilize nonlinear modes in multidimensional systems remains an important research topic. Generally, the simplest way is to modify the attractive cubic nonlinearity, which includes reducing the cubic nonlinearity to quadratic nonlinearity [2, 3], adding competitive nonlinearities, such as the competing cubic-quintic nonlinearity [4–10], changing cubic nonlinearity to saturable nonlinearity [11] or nonlocal nonlinearity [12–16].

Subsequently, one can introduce spin–orbit coupling to stabilize self-trapped modes, i.e., matter-wave solitons [17–26] and quantum droplets (QDs) [27]. QDs, a new type of self-bound quantum liquid state, were created experimentally in dipolar bosonic gases of dysprosium [28] and erbium [29], as well as in mixtures of two atomic states of ^{39}K [30] with contact interactions. QDs have attracted much attention in the field of ultracold atoms [31–61], which predicate a possibility in the framework of the 3D [31], 2D [32–38] and 1D [39–42] Gross–Pitaevskii (GP) equations. Research has shown that QDs have been formed with the help of zero-point quantum fluctuations, which can arrest the collapse of attractive Bose gases in two and three dimensions and can be described theoretically by the Lee–Huang–Yang (LHY) correction [62]. The LHY correction is proportional to $n^{5/2}$ in 3D [31] and $n^2 \ln(n/\sqrt{e})$ in 2D [32], where n is the condensate density, which plays an important role in stabilizing QDs. In these studies, in the 2D and 3D domains, the LHY term acts as a higher-order nonlinear repulsive interaction in the relative GP equations, which arrest the collapse of attractive Bose gases induced by the mean-field force.

Another possibility for the stabilization of nonlinear modes was revealed in BECs, which are trapped in an optical lattice [63]. Numerous studies have shown that BECs trapped in an optical lattice provide an ideal and clean platform for studying the nonlinear modes and their dynamics. In the optical lattice, various types of matter-wave solitons were investigated both numerically and analytically [64–78]. A potentially interesting research direction is to study QDs in a lattice. Recently, dynamics of QDs in a 1D optical lattice were studied [41, 79], and it was found that the optical lattice potential strongly influences the stability of the QDs, and this system can support stable dipole-model QDs in a very small range of proper parameters. In the 2D or 3D domains, optical lattices can

*These authors contributed equally to this work. arXiv: 2009.06804. This article can also be found at http://journal.hep.com.cn/fop/EN/10.1007/s11467-020-1011-3.

provide more freedom than their 1D counterparts. For example, in higher-dimensional spaces, we can construct more complex lattice structures, such as square lattices [80–87] and honeycomb lattices [88–91] (graphene structure). Furthermore, in the higher-dimensional domains, we can not only consider the fundamental or the dipole modes but also the quadrupole modes [92–96], or more interestingly, the vortex modes. However, the dynamics of QDs in these higher-dimensional spaces with periodic potential have not been considered thus far. It was known that periodic potential is a fundamental problem in solid-state physics. The combination of QDs and lattice potential may open an avenue to study the dynamics of such new kind of liquid in some advanced topic of condense matter physics, such as discrete systems and topological objects.

The objective of the present work is to demonstrate the possibility of creating stable zero-vorticity and vortex LQDs in BECs, which are trapped in a 2D optical square lattice, and study their characteristics. Similar to their 1D counterparts, two types of LQDs, viz., onsite-centered and offsite-centered LQDs, the centers of which are located at the minimum and the maximum of the potential, respectively, are identified. The stability of these LQDs with zero-vorticity ($S = 0$) and a vortex with $S = 1$ are studied in detail. The rest of this paper is structured as follows: the model for the current system is described in Section 2, and the results of the 2D LQDs for $S = 0$ and 1 are discussed in detail in Section 3, and this work is concluded in Section 4.

2 The model

We assume that the LQDs, which are formed by binary BECs, are strongly confined in the transverse direction with lateral size $l \gg \sqrt{a_{\pm}a_{\perp}}$, where $a_{\pm}$ and $a_{\perp}$ are the self-repulsion scattering lengths of each component and the transverse confinement length, respectively. For the current experimental system, we can select the length of a single lattice site to be $D \sim 1\ \mu$m, $a_{\pm} \sim 3$ nm, and $a_{\perp} \ll 1\ \mu$m. This condition definitely holds for $l \sim 10D$. In this case, the GP equation with LHY correction is also reduced to 2D form for the scaled wave functions $\psi_{\pm}$ of the two components as

$$\begin{aligned} \mathrm{i}\partial_t\psi_{\pm} = & -\frac{1}{2}\nabla^2\psi_{\pm}+\frac{4\pi}{g}(|\psi_{\pm}|^2-|\psi_{\mp}|^2)\psi_{\pm}+V(x,y)\psi_{\pm} \\ & +(|\psi_{\pm}|^2+|\psi_{\mp}|^2)\psi_{\pm}\ln(|\psi_{\pm}|^2+|\psi_{\mp}|^2), \end{aligned} \tag{1}$$

where $g > 0$ is the coupling constant and $V(x, y)$ is the 2D lattice potential. Here, the logarithmic form of the LHY term has been adopted because of strong transverse confinement. If these two components are under a symmetric condition, i.e., $a_+ = a_-$, the mean-field self-repulsion and the cross-attraction between the binary BECs are canceled with each other, Eq. (1) can be further simplified by adopting the symmetric state $\psi_+ = \psi_- = \phi/\sqrt{2}$ as

$$\mathrm{i}\frac{\partial\phi}{\partial t} = -\frac{1}{2}\nabla^2\phi + V(x,y)\phi + |\phi|^2\ln|\phi|^2\phi. \tag{2}$$

The analysis in Ref. [36] has demonstrated that the energy of this LHY term can provide a minimum for supporting a QDs. Adding the lattice potential does not eliminate such an energy minimum, hence, the LQDs can formed in the current model.

Here, we use the square lattices as the potential; hence, $V(x, y)$ can be described as

$$V(x,y) = V_0\left[\cos^2\left(\frac{\pi}{D}x\right)+\cos^2\left(\frac{\pi}{D}y\right)\right] \tag{3}$$

or

$$V(x,y) = V_0\left[\sin^2\left(\frac{\pi}{D}x\right)+\sin^2\left(\frac{\pi}{D}y\right)\right], \tag{4}$$

where $V_0 < 0$ is the lattice modulation depth and D is the lattice constant (i.e., the period of the lattice). Refer to Ref. [97], the simplest way to form 1D lattices is by superimposing two oppositely directed laser beams with the same frequency, and may be produced in higher-dimensions by superimposing more than two beams with different wave vectors. We consider the case in which the polarizations of the beams propagating in the x-direction are the same, as are the polarizations of the beams propagating in the y-direction, but the polarization of the beams propagating in the two directions are orthogonal. The resulting potential energy becomes proportional to $\cos^2(qx)+\cos^2(qy)$ or $\sin^2(qx)+\sin^2(qy)$ and gives rise to a square lattice with lattice constant equal to $D = \lambda/2$. Even though there is no essential difference in the expressions in Eqs. (3) and (4) for square lattices, which feature only a $\pi/2$ phase shift, the two expressions in Eqs. (3) and (4) are crucial for the formation of the LQDs centered at the origin of the coordinates. Because we let $V_0 < 0$, the square lattice constructed by Eq. (3) at the origin of the coordinates is a local minimum of the potential, while the lattice constructing by Eq. (4) at the origin of the coordinates is a local maximum of the potential, which means that the square lattice constructed by Eq. (3) can provide a lattice site for the center of the droplets, while the lattice of Eq. (4) cannot. Therefore, we can use these two expressions, Eqs. (3) and (4), to characterize the two types of LQDs, which are centered at the minimum and the maximum of the potential, respectively. The former (the center located at the minimum of the potential) are called onsite-centered LQDs, and the latter (the center located at the maximum of the potential) are called offsite-centered LQDs. The total norm for these two types of LQDs can all be characterized as

$$N = \int\int |\phi|^2\,\mathrm{d}x\,\mathrm{d}y. \tag{5}$$

Stationary solutions to Eq. (2) with a chemical potential μ are sought as follows:

$$\phi(x,y,t) = \tilde{\phi}(x,y)\,\mathrm{e}^{-\mathrm{i}\mu t}, \tag{6}$$

where $\tilde{\phi}(x,y)$ represents the stationary wave function. Stationary LQDs with different topological charges S were produced by the imaginary-time-integration (ITM) method [98, 99] with an initial guess of

$$\phi_0(x,y,t) = CR^S \exp\left(\mathrm{i}S\theta - \alpha R^2\right), \tag{7}$$

where C and α are positive real numbers, R and θ are 2D polar coordinates. Then, the stability of the solutions was verified by direct simulations of Eq. (2) in real time, with 1% random noise is added in the amplitude given by solutions. The soliton is stable if its density profile remains unchanged throughout the simulations. Here, we provide some analysis of the variation of the size of LQDs depends on N. Assuming the LQDs have occupied many lattices, we can use $V_0/2$ to average the lattice potentials in Eqs. (3) and (4), hence, the GP equation in Eq. (2) becomes

$$\mathrm{i}\frac{\partial\phi}{\partial t} = -\frac{1}{2}\nabla^2\phi + \frac{1}{2}V_0\phi + |\phi|^2\ln|\phi|^2\phi. \tag{8}$$

The energy of the system is

$$E = \frac{1}{2}\int\int\left[|\nabla\phi|^2 + V_0|\phi|^2 + |\phi|^4\ln\left(\frac{|\phi|^2}{\sqrt{e}}\right)\right]\mathrm{d}x\,\mathrm{d}y. \tag{9}$$

According to Ref. [36], Eqs. (8) and (9) can give rise to flat-top LQDs if the Thomas–Fermi (TF) approximation is adopted, and a constant peak density $|\phi_p|^2$ can be produced. Hence, the total area of the LQDs can be estimated by

$$\mathcal{A} = \frac{N}{|\phi_p|^2}. \tag{10}$$

Assuming $\mathcal{A} \approx ns$, where s is the area per lattice site and n is the number of the lattices occupied by the LQDs, Eq. (10) becomes

$$n = \frac{N}{s|\phi_p|^2}, \tag{11}$$

which indicates that the total number of sites in the LQDs increases as N increases.

In the next section, we will study the effect of the optical lattice potential on the stationary LQDs in detail. For convenience, we fix the value of the lattice constant $D = 5$ in the numerical simulations. Hence, the free control parameters in the system are lattice modulation depth V_0 and the total norm of the LQDs N.

3 Numerical results

3.1 Zero-vorticity LQDs

Even though Eq. (11) demonstrates that the total number of sites of the LQDs increase as N increases for the onsite-centered LQDs and offsite-centered LQDs, the amounts of growth in n are different. Figure 1 shows the sketch maps of the growth pattern of the first 4 steps for these two types of LQDs. For the onsite-centered LQDs, the 1st step of its pattern occupies one lattice site (i.e., $n = 1$) at the origin of the coordinates. The next step is the extension from the center to the two sides in the x- and y-directions ($n = 5$). In the 3rd step, it occupies the four corners, and it becomes a 9-site square. Then, it continues to expand to the two sides in x- and y-directions in the 4th step and $n = 13$. For the offsite-centered LQDs, because the center are not occupied by a lattice site, the 1st step is a 4-site square shape with four closest lattice sites situated around the origin of the coordinates. Then, it expands to the two sides in the x- and y-directions in the 2nd step, and $n = 12$. In the 3rd step, the offsite-centered LQDs become a 16-site square shape again by filling the 4 corners. Then, it becomes $n = 24$ by keeping the expansion to the two sides in x- and y-directions in the 4th step. It is interesting to note that the number of sites for the zero-vorticity onsite-centered LQDs are odd, while the numbers of sites for the zero-vorticity offsite-centered LQDs are even. Following the above description, it is convenient to use the number of sites, n, to characterize the LQDs in the following study.

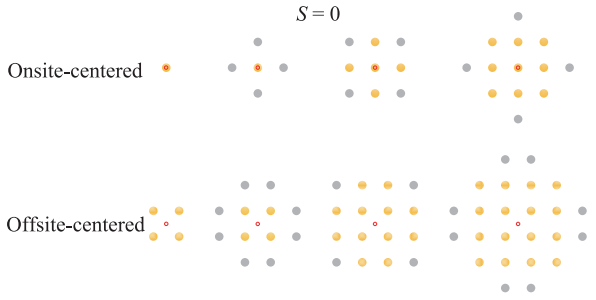

Fig. 1 The upper row is the sketch map of the growth pattern of onsite-centered LQDs ($S = 0$) versus n. The lower row is the same sketch map for offsite-centered LQDs. The red circles represent the centers of the LQDs.

The stationary solutions of the LQDs with different numbers of sites are carried out by numerically solving Eq. (2). The stabilities of the LQDs are identified by the direct simulation of Eq. (2) initialized with the solution by adding 1% random noise. Numerical studies found that the stability areas for the two types of LQDs, which are characterized by the number of sites, depend on total norm N and the modulation depth of the potential V_0. Figures 2(a, b) display the stability areas of the onsite-centered and offsite-centered LQDs, respectively, in steps $1 \to 3$ in the $(N, |V_0|)$ plane. According to Fig. 1, the number of sites for the onsite-centered LQDs are 1, 5, and 9, while the number of sites for the offsite-centered LQDs are 4, 12, and 16. Figures 2(a, b) show that these number as color stripes, which represent the stability areas of the LQDs for different numbers of sites, concentrated to the lower N area during the increase of $|V_0|$. Those

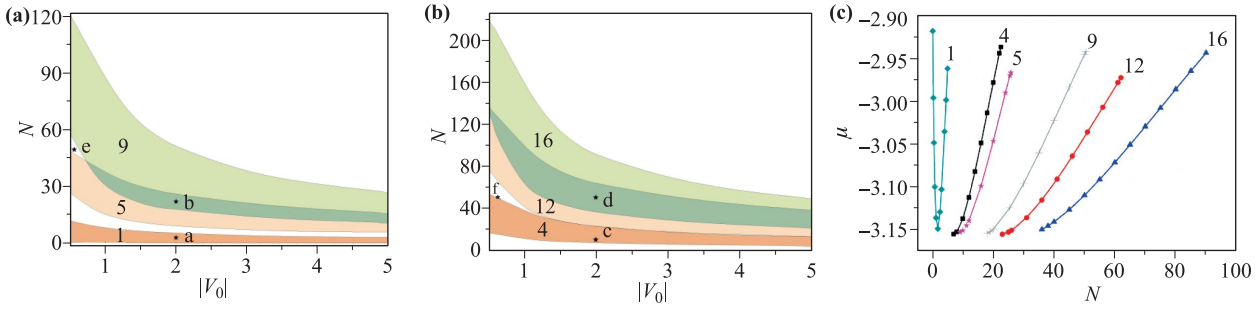

Fig. 2 **(a, b)** Stability areas of the minimum three LQDs with zero-vorticity, which correspond to 1, 5, and 9 sites for the onsite-centered LQDs and 4, 12, and 16 sites for the offsite-centered LQDs in the plane of $(N, |V_0|)$. The bistability states occur in the light green areas. **(c)** Chemical potential μ versus the total norm N, for stable onsite-centered and offsite-centered LQDs. Here, we fixed $V_0 = -2$.

phenomena can be explained as follow: the increase in the modulation depth decreases the effective area per lattice site (i.e., s), and according to Eq. (11), resulting in a corresponding increase in the growth rate of n versus N. Moreover, the concentration of these color stripes gives rise to the overlap between them [see the light green areas in Figs. 2(a, b)]. These areas of overlap allow the coexistence of the different numbers of sites with equal norm N and lattice modulation depth V_0.

Typical examples of the density patterns of the stable zero-vorticity onsite-centered and offsite-centered LQDs are shown in Fig. 3, which correspond to points "a, b, c, and d" in the stability areas in Figs. 2(a, b). The parameters are $(N, V_0) = (3, -2)$, $(22, -2)$, $(10, -2)$, and $(50, -2)$, respectively. Note that the LQDs in Figs. 3(a2, a3) and (b2, b3) are selected from the bistable areas, which allows the coexistence of different numbers of sites with equal norms and lattice modulation depths, see the points "b" and "d" in Figs. 2(a, b), respectively. It is worth noting that there are some other LQDs solutions, which are not symmetric to the origin of the coordinate are found outside the color stripe areas, i.e., the blank region. Typical examples of these types of LQDs are shown in Fig. 4, which correspond to points "e and f" in the blank areas in Figs. 2(a, b). As seen from the evolution figure [Figs. 4(a2, b2)], these types of LQDs are also stable. Obviously, these types of LQDs cannot be characterized by the expansion law in Fig. 1; these types will not be discussed in detail in

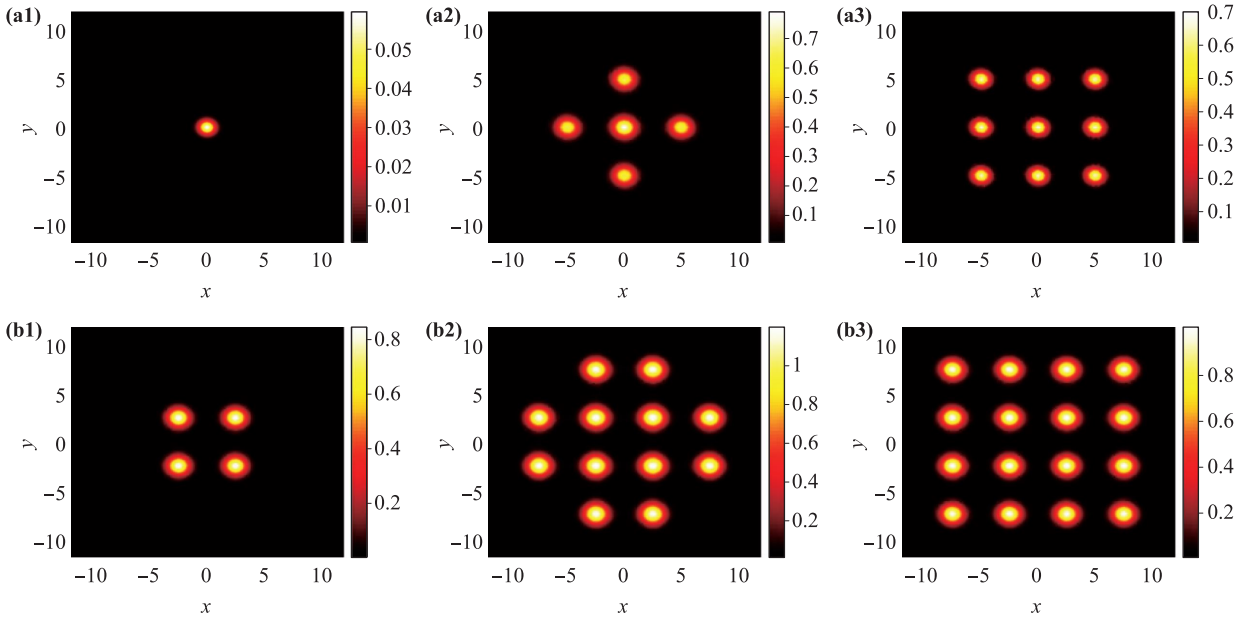

Fig. 3 Typical examples of the density patterns of the stable onsite-centered (a1–a3) and offsite-centered (b1–b3) LQDs with zero-vorticity, which correspond to points "a, b, c, and d" in the stability areas in Fig. 2. The parameters are $(N, V_0) = (3, -2)$, $(22, -2)$, $(10, -2)$, and $(50, -2)$, respectively. Here, the LQDs in (a2, a3) and (b2, b3) are selected from the bistable areas [see the points "b" and "d" in Figs. 2(a, b) respectively].

the current paper.

Figure 2(c) displays the dependence of the chemical potential μ and the total norm N, for stable onsite-centered and offsite-centered LQDs, here, we fixed $V_0 = -2$. The results indicate that only the $\mu(N)$ curves for $n = 1$ (onsite-centered LQDs) satisfy $\mathrm{d}\mu/\mathrm{d}N < 0$ when $N < 1.8$, which is well known as the Vakhitov–Kolokolov (VK) criterion (the necessary stability condition for a soliton in the attractive background). However, when $N > 1.8$, the $\mu(N)$ curves for the LQDs with all the numbers of sites satisfy $\mathrm{d}\mu/\mathrm{d}N > 0$, which seems to violate the VK criterion. The similar results were previously reported in 1D model and the simulations have demonstrated that both soliton branches are stable in the CQ-nonlinear channel [100]. While, in 2D model, which combines a checkerboard potential, alias the Kronig–Penney lattice, with the self-focusing cubic and self-defocusing quintic nonlinear terms, the branchs of each bistable solitons are stable against arbitrary perturbations [101]. Next, we will provide the analysis to explain why the $\mu(N)$ curves for these LQDs can violate the VK criterion.

According to Eq. (8), the stationary solution in the vicinity of ϕ_p obeys the stationary GP equation as follows:

$$\mu\phi_p = \frac{V_0}{2}\phi_p + \phi_p|\phi_p|^2\ln|\phi_p|^2. \tag{12}$$

Here, we have applied the TF approximation in Eq. (12). According to Eq. (10), the total ϕ_p can be expressed as $|\phi_p|^2 \approx N/\mathcal{A}$. Therefore, the chemical potential μ obeys

$$\mu = \frac{V_0}{2} + \frac{N}{\mathcal{A}}\ln\frac{N}{\mathcal{A}}. \tag{13}$$

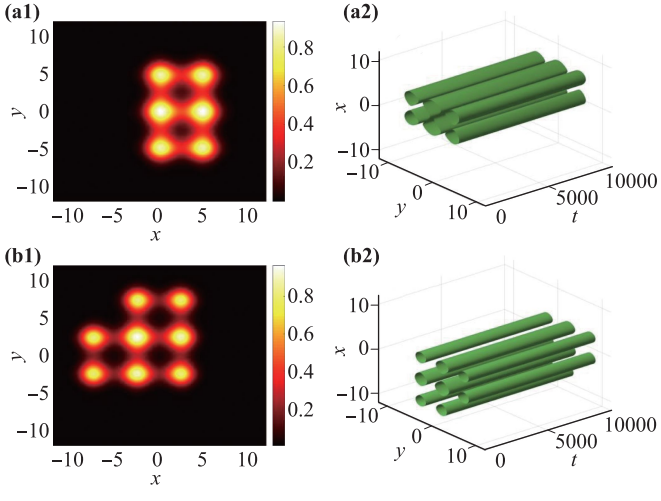

Fig. 4 Typical examples of some other LQDs solutions in the white region, which are not symmetric to the origin of the coordinates, whose parameters are $(N, V_0) = (49.4, -0.56)$ in (a1 and a2) and $(50.5, -0.7)$ in (b1 and b2), which correspond to points "e and f" in the blank areas in Figs. 2(a, b).

Hence,

$$\frac{\mathrm{d}\mu}{\mathrm{d}N} = \frac{1}{\mathcal{A}}\left(\ln\frac{N}{\mathcal{A}} + 1\right), \tag{14}$$

From Eq. (14), when $\ln(N/\mathcal{A}) + 1 > 0$, i.e., $N > \mathcal{A}/e$, we can obtain

$$\frac{\mathrm{d}\mu}{\mathrm{d}N} > 0. \tag{15}$$

So, above analysis demonstrate the $\mu(N)$ function for these LQDs can violate the VK criterion. In our simulations, we choose the lattice constant $D = 5$, so the area per lattice site $s = \pi(D/4)^2 \approx 4.91$, hence, $\mathcal{A} = 1 * s = 4.91$, yields, $N_{cr\_th} = \mathcal{A}/e = 1.806$. From Fig. 2(c), it can be seen that the numerical results ($N = 1.8$) are basically in agreement with the theoretical prediction ($N_{cr\_th} \approx 1.806$).

3.2 Vortex LQDs with $S = 1$

Whether the stable vortex LQDs can be found in current systems is a nontrivial issue. Generally, a vortical mode must have a density pivot at its center. Hence, for the onsite-centered vortex LQDs, their center lattice site will be occupied by the pivot. For offsite-center vortex LQDs, because the density of their center is already zero, it is not necessary to provide a lattice site to the density pivot. Fig. 5 shows the sketch maps of the growth patterns of the first 4 steps for the two types of vortex LQDs. For the onsite-centered vortex LQDs, because the central lattice site is already occupied by the density pivot, the 1st step of its pattern occupies the 4 closest lattice sites (i.e., $n = 4$) at the origin of the coordinates. Then, it expands to $n = 8$, 12, and 20 in the next 3 steps. This process is similar to the zero-vorticity case starting from the 2nd step with the central lattice site being removed. For the offsite-centered vortex LQDs, because the density is zero at the center, the expansion law is the same as that in the zero-vorticity case in Fig. 1. Thus, we can see that the offsite-centered LQDs with zero-vorticity and

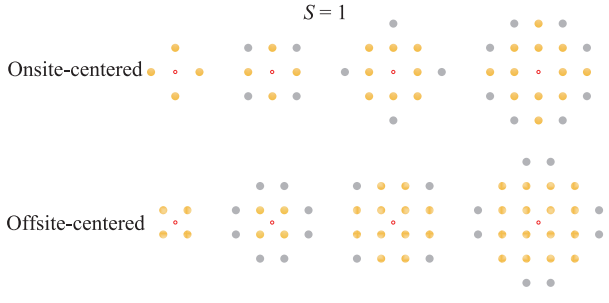

Fig. 5 The upper row is the sketch map of the growth pattern of onstie-centered LQDs with $S = 1$ versus n. The lower row is the same sketch map for offsite-centered LQDs. The red circles represent the centers of the LQDs.

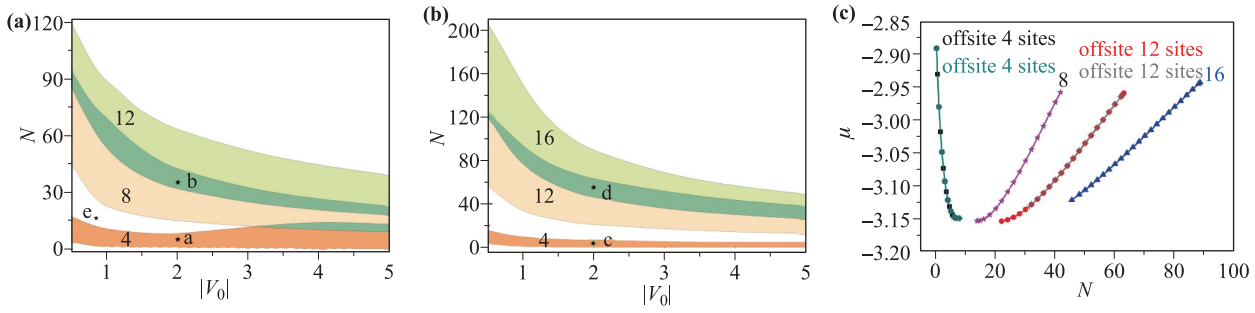

Fig. 6 **(a, b)** Stability area of the three minimum isotropic vortex LQDs with $S = 1$, which correspond to 4, 8, and 12 sites for the onsite-centered LQDs and 4, 12, and 16 sites for the offsite-centered LQDs in the plane of $(N, |V_0|)$. The bistability states occur in the light green areas. **(c)** Chemical potential μ versus the total norm N, for the stable onsite-centered and offsite-centered LQDs. Here, we fixed $V_0 = -2$.

vortex LQDs with $S = 1$ are heterogeneous, which means that they occupy the same lattices with the same density pattern, but have different amplitude and phase distribution. It is also interesting to find that the numbers of sites are even for both the onsite-centerred and offsite-centered types. In the following discussion, we will continue to use the number of sites to characterize the vortex LQDs.

Numerical results show that stable vortex LQDs with $S = 1$ exist in our systems. Similar to LQDs with zero-vorticity, we plot their stability areas with different colors in the $(N, |V_0|)$ plane in Figs. 6(a, b). Similar to the discussion above regarding zero-vorticity, these color stripes concentrate with increasing modulation depth $|V_0|$. Hence, the overlaps between them, which are labeled by the light green areas, also appear. Typical examples of the density patterns of the stable onsite-centered (a1–a3)

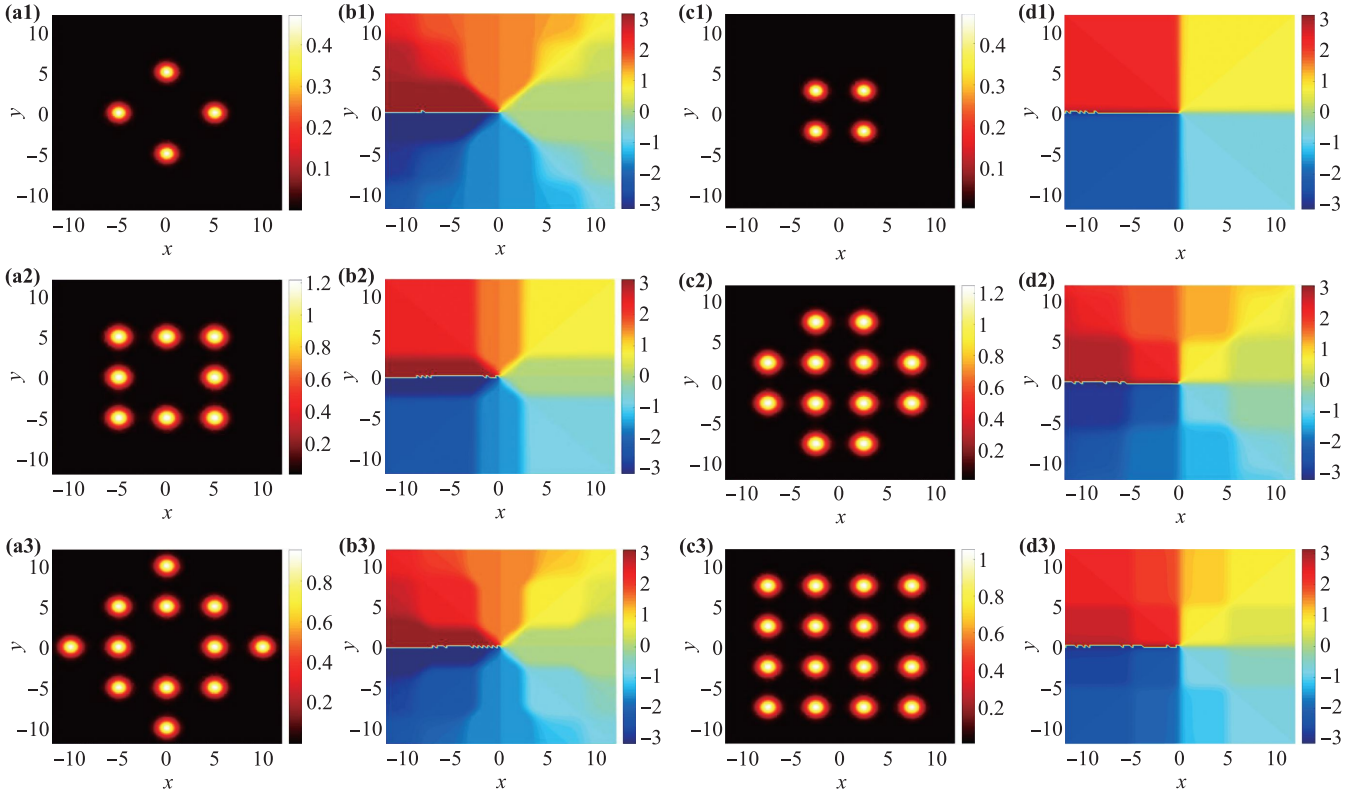

Fig. 7 Typical examples of the density patterns of the stable onsite-centered (a1–a3) and offsite-centered (c1–c3) vortex LQDs with $S = 1$, which correspond to points "a, b, c, and d" in the stability areas in Fig. 6. The parameters are $(N, V_0) = (5, -2)$, $(35, -2)$, $(5, -2)$, and $(55, -2)$, respectively. (b1–b3) and (d1–d3) show the corresponding phase patterns of (a1–a3) and (c1–c3), respectively. Here, the LQDs in (a2,a3) and (c2,c3) are selected from the bistable areas [see the points "b" and "d" in Figs. 6(a, b) respectively].

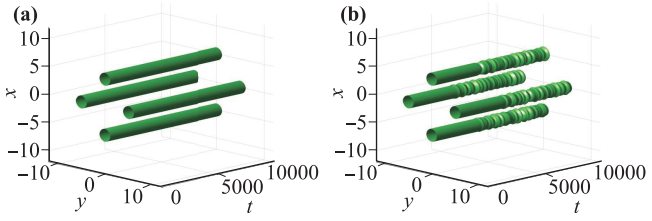

Fig. 8 **(a)** Direct simulations of the evolution of stable onsite-centered vortex LQDs with $S = 1$, which correspond to point "a" in the stability areas in Fig. 6(a). **(b)** Typical examples of unstable LQDs in the white region, which correspond to point "e" in the stability areas in Fig. 6(a), and parameters are $(N, V_0) = (15, -1)$.

and offsite-centered (c1–c3) vortex LQDs with $S = 1$ are shown in Fig. 7, which correspond to points "a, b, c, and d" in the stability areas in Figs. 6(a, b). The LQDs in (a2, a3) and (c2, c3) are selected from the bistable areas, which allows the coexistence of different numbers of sites with equal norms and lattice modulation depths, see the points "b" and "d" in Figs. 6(a, b) respectively. Figures. 7(b1–b3, d1–d3) show the corresponding phase patterns. Here, we fixed the lattice modulation depth $V_0 = -2$. Outside the color areas, unstable vortex LQDs may be found. Typical examples of the evolution of the stable and unstable vortex LQDs are shown in Fig. 8, which correspond to points "a" and "e", respectively, in the stability areas in Fig. 6(a).

Figure 6(c) displays the dependence of the chemical potential μ and the total norm N, for stable onsite-centered and offsite-centered vortex LQDs. Here we fixed $V_0 = -2$. It is worth noting that the two types of LQDs with the same numbers of sites will have equal chemical potentials at the same norm N [see Fig. 6(c), the 4-site and 12-site onsite-centered and offsite-centered vortex LQDs, respectively]. This phenomenon indicates that at the same norm N, these two types of LQDs with the same numbers of sites are degenerate states. This phenomenon is different from the LQDs with zero-vorticity. Next, as with the zero-vorticity LQDs, the dependencies between the chemical potential μ and the total norm N, does not necessarily satisfy the VK criterion.

4 Conclusion

In this paper, we studied two-dimensional (2D) lattice quantum droplets (LQDs) trapped in 2D optical lattices. First, we demonstrated the possibility of creating stable zero-vorticity and vortex LQDs and then investigated the influence of the optical lattice potential on the LQDs. We found two types of stable LQDs: onsite-centered and offsite-centered LQDs. Furthermore, the stability areas of the two types of zero-vorticity LQDs and vortex QDs with $S = 1$ are given. Bistability characteristics are shown in a stable region diagram, which allows the coexistence of different numbers of sites with equal norms and lattice modulation depths. Then, we found that some other zero-vorticity LQDs are stable in the blank region. Different from the zero-vorticity LQDs, the μ–N relationship shows that the two types of vortex LQDs with the same number of sites are degenerated. An important point is that for stable LQDs with a fixed number of sites, the dependencies between the chemical potential μ and the total norm N, can violate the Vakhitov–Kolokolov (VK) criterion.

The present analysis can be extended in some directions. First, the current study is based only on square lattices, and we can extend it to other lattice structures, such as triangle lattices or graphene structures. The latter option may be able to relate the LQDs to topological phenomena. Further, for the vortices, it is worth considering whether hidden vortices and anisotropic vortices can be supported by the lattice. Finally, a challenging option is to seek stable vortex LQDs in the 3D configuration.

Acknowledgements This work was supported by the National Natural Science Foundation of China (NNSFC) through Grant Nos. 11905032 and 11874112, the Key Research Projects of General Colleges in Guangdong Province through Grant No. 2019KZDXM001, the Foundation for Distinguished Young Talents in Higher Education of Guangdong through Grant No. 2018KQNCX279, and the Special Funds for the Cultivation of Guangdong College Students Scientific and Technological Innovation (No. xsjj202005zra01).

References

1. L. D. Landau and E. M. Lifshitz, Quantum Mechanics: Nonrelativistic Theory, Moscow: Nauka publishers, 1974
2. W. E. Torruellas, Z. Wang, D. J. Hagan, E. W. VanStryland, G. I. Stegeman, L. Torner, and C. R. Menyuk, Observation of two-dimensional spatial solitary waves in a quadratic medium, *Phys. Rev. Lett.* 74(25), 5036 (1995)
3. X. Liu, K. Beckwitt, and F. Wise, Two-dimensional optical spatiotemporal solitons in quadratic media, *Phys. Rev. E* 62(1), 1328 (2000)
4. D. Mihalache, D. Mazilu, L. C. Crasovan, B. A. Malomed, and F. Lederer, Three-dimensional spinning solitons in the cubic–quintic nonlinear medium, *Phys. Rev. E* 61(6), 7142 (2000)
5. S. Konar, M. Mishra, and S. Jana, Nonlinear evolution of cosh-Gaussian laser beams and generation of flat top spatial solitons in cubic–quintic nonlinear media, *Phys. Lett. A* 362(5–6), 505 (2007)
6. E. L. Falcão-Filho, C. B. de Araújo, G. Boudebs, H. Leblond, and V. Skarka, Robust two-dimensional spatial solitons in liquid carbon disulfide, *Phys. Rev. Lett.* 110(1), 013901 (2013)
7. Y. Y. Wang, L. Chen, C. Q. Dai, J. Zheng, and Y. Fan, Exact vector multipole and vortex solitons in the media with spatially modulated cubic–quintic nonlinearity, *Nonlinear Dyn.* 90(2), 1269 (2017)

8. C. Q. Dai, R. P. Chen, Y. Y. Wang, and Y. Fan, Dynamics of light bullets in inhomogeneous cubic–quantic-septimal nonlinear media with *PT*-symmetric potentials, *Nonlinear Dyn.* 87(3), 1675 (2017)
9. Y. Chen, L. Zheng, and F. Xu, Spatiotemporal vector and scalar solitons of the coupled nonlinear Schr inger equation with spatially modulated cubic–quantic-septimal nonlinearities, *Nonlinear Dyn.* 93(4), 2379 (2018)
10. J. Li, Y. Zhu, J. Han, W. Qin, C. Dai, and S. Wang, Scalar and vector multipole and vortex solitons in the spatially modulated cubic–quintic nonlinear media, *Nonlinear Dyn.* 91(2), 757 (2018)
11. M. Segev, G. C. Valley, B. Crosignani, P. DiPorto, and A. Yariv, Steady-state spatial screening solitons in photorefractive materials with external applied field, *Phys. Rev. Lett.* 73(24), 3211 (1994)
12. M. Peccianti, K. A. Brzdakiewicz, and G. Assanto, Nonlocal spatial soliton interactions in nematic liquid crystals, *Opt. Lett.* 27(16), 1460 (2002)
13. P. Pedri and L. Santos, Two-dimensional bright solitons in dipolar Bose–Einstein condensates, *Phys. Rev. Lett.* 95(20), 200404 (2005)
14. I. Tikhonenkov, B. A. Malomed, and A. Vardi, Anisotropic solitons in dipolar Bose–Einstein condensates, *Phys. Rev. Lett.* 100(9), 090406 (2008)
15. J. Huang, X. Jiang, H. Chen, Z. Fan, W. Pang, and Y. Li, Quadrupolar matter-wave soliton in two-dimensional free space, *Front. Phys.* 10(4), 100507 (2015)
16. F. Maucher, N. Henkel, M. Saffman, W. Królikowski, S. Skupin, and T. Pohl, Rydberg-induced solitons: Three-dimensional self-trapping of matter waves, *Phys. Rev. Lett.* 106(17), 170401 (2011)
17. Y. Xu, Y. Zhang, and C. Zhang, Bright solitons in a two-dimensional spin–orbit-coupled dipolar Bose–Einstein condensate, *Phys. Rev. A* 92(1), 013633 (2015)
18. X. Jiang, Z. Fan, Z. Chen, W. Pang, Y. Li, and B. A. Malomed, Two-dimensional solitons in dipolar Bose–Einstein condensates with spin–orbit coupling, *Phys. Rev. A* 93(2), 023633 (2016)
19. Y. Li, Y. Liu, Z. Fan, W. Pang, S. Fu, and B. A. Malomed, Two-dimensional dipolar gap solitons in free space with spin–orbit coupling, *Phys. Rev. A* 95(6), 063613 (2017)
20. X. Chen, Z. Deng, X. Xu, S. Li, Z. Fan, Z. Chen, B. Liu, and Y. Li, Nonlinear modes in spatially confined spin–orbit-coupled Bose–Einstein condensates with repulsive nonlinearity, *Nonlinear Dyn.* 101(1), 569 (2020)
21. Z. Ye, Y. Chen, Y. Zheng, X. Chen, and B. Liu, Symmetry breaking of a matter-wave soliton in a double-well potential formed by spatially confined spin–orbit coupling, *Chaos Solitons Fractals* 130, 109418 (2020)
22. B. Liu, R. Zhong, Z. Chen, X. Qin, H. Zhong, Y. Li, and B. A. Malomed, Holding and transferring matter-wave solitons against gravity by spin–orbit-coupling tweezers, *New J. Phys.* 22(4), 043004 (2020)
23. B. Liao, S. Li, C. Huang, Z. Luo, W. Pang, H. Tan, B. A. Malomed, and Y. Li, Anisotropic semi-vortices in dipolar spinor condensates controlled by Zeeman splitting, *Phys. Rev. A* 96(4), 043613 (2017)
24. B. Liao, Y. Ye, J. Zhuang, C. Huang, H. Deng, W. Pang, B. Liu, and Y. Li, Anisotropic solitary semi-vortices in dipolar spinor condensates controlled by the two-dimensional anisotropic spin–orbit coupling, *Chaos Solitons Fractals* 116, 424 (2018)
25. S. Liu, B. Liao, J. Kong, P. Chen, J. Lü, Y. Li, C. Huang, and Y. Li, Anisotropic semi vortices in spinor dipolar Bose–Einstein condensates induced by mixture of Rashba–Dresselhaus coupling, *J. Phys. Soc. Jpn.* 87(9), 094005 (2018)
26. W. Pang, H. Deng, B. Liu, J. Xu, and Y. Li, Two-dimensional vortex solitons in spin–orbit-coupled dipolar Bose–Einstein condensates, *Appl. Sci. (Basel)* 8(10), 1771 (2018)
27. X. Cui, Spin–orbit-coupling-induced quantum droplet in ultracold Bose–Fermi mixtures, *Phys. Rev. A* 98(2), 023630 (2018)
28. M. Schmitt, M. Wenzel, F. Böttcher, I. Ferrier-Barbut, and T. Pfau, Self-bound droplets of a dilute magnetic quantum liquid, *Nature* 539(7628), 259 (2016)
29. L. Chomaz, S. Baier, D. Petter, M. J. Mark, F. Wächtler, L. Santos, and F. Ferlaino, Quantum-fluctuation-driven crossover from a dilute Bose–Einstein condensate to a macrodroplet in a dipolar quantum fluid, *Phys. Rev. X* 6(4), 041039 (2016)
30. C. R. Cabrera, L. Tanzi, J. Sanz, B. Naylor, P. Thomas, P. Cheiney, and L. Tarruell, Quantum liquid droplets in a mixture of Bose–Einstein condensates, *Science* 359(6373), 301 (2018)
31. D. S. Petrov, Quantum mechanical stabilization of a collapsing Bose–Bose mixture, *Phys. Rev. Lett.* 115(15), 155302 (2015)
32. D. S. Petrov and G. E. Astrakharchik, Ultradilute low-dimensional liquids, *Phys. Rev. Lett.* 117(10), 100401 (2016)
33. P. Zin, M. Pylak, T. Wasak, M. Gajda, and Z. Idziaszek, Quantum Bose–Bose droplets at a dimensional crossover, *Phys. Rev. A* 98, 051603(R) (2018)
34. Y. Li, Z. Luo, Y. Liu, Z. Chen, C. Huang, S. Fu, H. Tan, and B. A. Malomed, Two-dimensional solitons and quantum droplets supported by competing self- and cross-interactions in spin–orbit-coupled condensates, *New J. Phys.* 19(11), 113043 (2017)
35. T. Ilg, J. Kumlin, L. Santos, D. S. Petrov, and H. P. Büchler, Dimensional crossover for the beyond-mean-field correction in Bose gases, *Phys. Rev. A* 98(5), 051604 (2018)
36. Y. Li, Z. Chen, Z. Luo, C. Huang, H. Tan, W. Pang, and B. A. Malomed, Two-dimensional vortex quantum droplets, *Phys. Rev. A* 98(6), 063602 (2018)
37. X. Zhang, X. Xu, Y. Zheng, Z. Chen, B. Liu, Ch. Huang, B. A. Malomed, and Y. Li, Semidiscrete quantum droplets and vortices, *Phys. Rev. Lett.* 123(13), 133901 (2019)
38. Z. Lin, X. Xu, Z. Chen, Z. Yan, Z. Mai, and B. Liu, Two-dimensional vortex quantum droplets get thick, *Commun. Nonlinear Sci. Numer. Simul.* 93, 105536 (2020)

39. B. Liu, H. Zhang, R. Zhong, X. Zhang, X. Qin, X. Huang, Y. Li, and B. A. Malomed, Symmetry breaking of quantum droplets in a dual-core trap, *Phys. Rev. A* 99(5), 053602 (2019)

40. G. E. Astrakharchik and B. A. Malomed, Dynamics of one-dimensional quantum droplets, *Phys. Rev. A* 98(1), 013631 (2018)

41. Zh. Zhou, X. Yu, Y. Zou, and H. Zhong, Dynamics of quantum droplets in a one-dimensional optical lattice, *Commun. Nonlinear Sci. Numer. Simul.* 78, 104881 (2019)

42. Zh. Zhou, B. Zhu, H. Wang, and H. Zhong, Stability and collisions of quantum droplets in *PT*-symmetric dual-core couplers, *Commun. Nonlinear Sci. Numer. Simul.* 91, 105424 (2020)

43. F. Wächtler and L. Santos, Quantum filaments in dipolar Bose–Einstein condensates, *Phys. Rev. A* 93, 061603(R) (2016)

44. F. Wächtler and L. Santos, Ground-state properties and elementary excitations of quantum droplets in dipolar Bose–Einstein condensates, *Phys. Rev. A* 94(4), 043618 (2016)

45. D. Baillie, R. M. Wilson, R. N. Bisset, and P. B. Blakie, Self-bound dipolar droplet: A localized matter wave in free space, *Phys. Rev. A* 94, 021602(R) (2016)

46. D. Edler, C. Mishra, F. Wächtler, R. Nath, S. Sinha, and L. Santos, Quantum fluctuations in quasi-one-dimensional dipolar Bose–Einstein condensates, *Phys. Rev. Lett.* 119(5), 050403 (2017)

47. I. Ferrier-Barbut, H. Kadau, M. Schmitt, M. Wenzel, and T. Pfau, Observation of quantum droplets in a strongly dipolar Bose gas, *Phys. Rev. Lett.* 116(21), 215301 (2016)

48. I. Ferrier-Barbut, M. Wenze, F. Böttcher, T. Langen, M. Isoard, S. Stringari, and T. Pfau, Scissors mode of dipolar quantum droplets of dysprosium atoms, *Phys. Rev. Lett.* 120(16), 160402 (2018)

49. A. Cidrim, F. E. A. dos Santos, E. A. L. Henn, and T. Macrí, Vortices in self-bound dipolar droplets, *Phys. Rev. A* 98(2), 023618 (2018)

50. R. N. Bisset, R. M. Wilson, D. Baillie, and P. B. Blakie, Ground-state phase diagram of a dipolar condensate with quantum fluctuations, *Phys. Rev. A* 94(3), 033619 (2016)

51. Y. Sekino and Y. Nishida, Quantum droplet of one-dimensional bosons with a three-body attraction, *Phys. Rev. A* 97, 011602(R) (2018)

52. C. Staudinger, F. Mazzanti, and R. E. Zillich, Self-bound Bose mixtures, *Phys. Rev. A* 98(2), 023633 (2018)

53. V. Cikojević, K. Dželalija, P. Stipanović, and L. V. Markić, Ultradilute quantum liquid drops, *Phys. Rev. B* 97, 140502(R) (2018)

54. P. Cheiney, C. R. Cabrera, J. Sanz, B. Naylor, L. Tanzi, and L. Tarruell, Bright soliton to quantum droplet transition in a mixture of Bose–Einstein condensates, *Phys. Rev. Lett.* 120(13), 135301 (2018)

55. G. Semeghini, G. Ferioli, L. Masi, C. Mazzinghi, L. Wolswijk, F. Minardi, M. Modugno, G. Modugno, M. Inguscio, and M. Fattori, Self-bound quantum droplets in atomic mixtures, *Phys. Rev. Lett.* 120(23), 235301 (2018)

56. A. Cappellaro, T. Macrì, and L. Salasnich, Collective modes across the soliton–droplet crossover in binary Bose mixtures, *Phys. Rev. A* 97(5), 053623 (2018)

57. A. Pricoupenko and D. S. Petrov, Dimer–dimer zero crossing and dilute dimerized liquid in a one-dimensional mixture, *Phys. Rev. A* 97(6), 063616 (2018)

58. A. Cappellaro, T. Macrí, G. F. Bertacco, and L. Salasnich, Equation of state and self-bound droplet in Rabi-coupled Bose mixtures, *Sci. Rep.* 7(1), 13358 (2017)

59. N. Westerberg, K. E. Wilson, C. W. Duncan, D. Faccio, E. M. Wright, P. Öhberg, and M. Valiente, Self-bound droplets of light with orbital angular momentum, *Phys. Rev. A* 98(5), 053835 (2018)

60. E. Shamriz, Zh. Chen, B. A. Malomed, and H. Sakaguchi, Singular mean-field states: A brief review of recent results, *Condens. Matter* 5, 20 (2020)

61. Z. Luo, W. Pang, B. Liu, Y. Li, and A. B. Malomed, A new form of liquid matter: Quantum droplets, *Front. Phys.* (2021) (submitted), arXiv: 2009.01061

62. T. D. Lee, K. S. Huang, and C. N. Yang, Eigenvalues and eigenfunctions of a Bose system of hard spheres and its low-temperature properties, *Phys. Rev.* 106(6), 1135 (1957)

63. O. Morsch and M. Oberthaler, Dynamics of Bose–Einstein condensates in optical lattices, *Rev. Mod. Phys.* 78(1), 179 (2006)

64. H. Zhang, F. Chen, C. Yu, L. Sun, and D. Xu, Tunable ground-state solitons in spin–orbit coupling Bose–Einstein condensates in the presence of optical lattices, *Chin. Phys. B* 26(8), 080304 (2017)

65. R. Campbell, and G. L. Oppo, Stationary and traveling solitons via local dissipation in Bose–Einstein condensates in ring optical lattices, *Phys. Rev. A* 94(4), 043626 (2016)

66. X. Zhu, H. Li, Z. Shi, Y. Xiang, and Y. He, Gap solitons in spin–orbit-coupled Bose–Einstein condensates in mixed linear–nonlinear optical lattices, *J. Phys. At. Mol. Opt. Phys.* 50(15), 155004 (2017)

67. F. Li, F. Zong, and Y. Wang, Vortical solitons of three-dimensional Bose–Einstein condensates under both a bichromatic optical lattice and anharmonic potentials, *Chin. Phys. Lett.* 30(6), 060306 (2013)

68. Sh. Chen, Q. Guo, S. Xu, M. R. Belić, Y. Zhao, D. Zhao, and J. He, Vortex solitons in Bose–Einstein condensates with spin–orbit coupling and Gaussian optical lattices, *Appl. Math. Lett.* 92, 15 (2019)

69. Z. He, Z. Zhang, Sh. Zhu, and W. Liu, Oscillation and fission behavior of bright–bright solitons in two-species Bose–Einstein condensates trapped in an optical potential, *Acta Physica Sinica* 63, 190502 (2014)

70. Z. Li and Q. Li, Dark soliton interaction of spinor Bose–Einstein condensates in an optical lattice, *Ann. Phys.* 322(8), 1961 (2007)

71. Ch. Song, J. Li, and F. Zong, Dynamic stability and manipulation of bright matter-wave solitons by optical lattices in Bose–Einstein condensates, *Chin. Phys. B* 21(2), 020306 (2012)
72. Z. D. Li, P. B. He, L. Li, J. Q. Liang, and W. M. Liu, Magnetic soliton and soliton collisions of spinor Bose–Einstein condensates in an optical lattice, *Phys. Rev. A* 71(5), 053611 (2005)
73. A. Muñoz Mateo, V. Delgado, M. Guilleumas, R. Mayol, and J. Brand, Nonlinear waves of Bose–Einstein condensates in rotating ring-lattice potentials, *Phys. Rev. A* 99(2), 023630 (2019)
74. X. Zhao, Y. Zhang, and W. Liu, Magnetic excitation of ultra-cold atoms trapped in optical lattice, *Acta Physica Sinica* 68, 043703 (2019)
75. G. Verma, U. D. Rapol, and R. Nath, Generation of dark solitons and their instability dynamics in two-dimensional condensates, *Phys. Rev. A* 95(4), 043618 (2017)
76. Z. Fan, J. Mai, Z. Chen, M. Xie, and Z. Luo, Matter-wave soliton buffer realized by a tailored one-dimensional lattice, *Mod. Phys. Lett. B* 32(06), 1850070 (2018)
77. H. Li, S. Xu, M. R. Belić, and J. Cheng, Three-dimensional solitons in Bose–Einstein condensates with spin–orbit coupling and Bessel optical lattices, *Phys. Rev. A* 98(3), 033827 (2018)
78. Z. Zhou, H. Zhong, B. Zhu, F. Xiao, K. Zhu, and J. Tan, Collision dynamics of dissipative matter-wave solitons in a perturbed optical lattice, *Chin. Phys. Lett.* 33(11), 110301 (2016)
79. L. Dong, W. Qi, P. Peng, L. Wang, H. Zhou, and C. Huang, Multi-stable quantum droplets in optical lattice, *Nonlinear Dynamics*, 2020
80. A. Mock, Paritytime-symmetry breaking in two-dimensional photonic crystals: Square lattice, *Phys. Rev. A* 93(6), 063812 (2016)
81. L. Salasnich and F. Toigo, Pair condensation in the BCS–BEC crossover of ultracold atoms loaded onto a two-dimensional square lattice, *Phys. Rev. A* 86(2), 023619 (2012)
82. R. Zaera, J. Vila, J. Fernandez-Saez, and M. Ruzzene, Propagation of solitons in a two-dimensional nonlinear square lattice, *Int. J. Non-linear Mech.* 106, 188 (2018)
83. Zh. Niu, Y. Tai, J. Shi, and W. Zhang, Bose–Einstein condensates in an eightfold symmetric optical lattice, *Chin. Phys. B* 29(5), 056103 (2020)
84. H. Chen, Y. Liu, Q. Zhang, Y. Shi, W. Pang, and Y. Li, Dipolar matter-wave solitons in two-dimensional anisotropic discrete lattices, *Phys. Rev. A* 93(5), 053608 (2016)
85. Y. Gao and S. Chu, Optical induction of non-diffracting discrete photonic lattice, *Superlattices Microstruct.* 78, 163 (2015)
86. K. Xie, A. D. Boardman, Q. Li, Z. Shi, H. Jiang, H. Xia, Z. Hu, J. Zhang, W. Zhang, Q. Mao, L. Hu, T. Yang, F. Wen, and E. Wang, Spatial algebraic solitons at the Dirac point in optically induced nonlinear photonic lattices, *Opt. Express* 25(24), 30349 (2017)
87. M. Metcalf, G. Chern, M. D. Ventra, and C. Chien, Matter-wave propagation in optical lattices: Geometrical and flat-band effects, *J. Phys. At. Mol. Opt. Phys.* 49(7), 075301 (2016)
88. D. Zhang, Y. Zhang, Z. Zhang, N. Ahmed, Y. Zhang, F. Li, M. R. Belić, and M. Xiao, Unveiling the link between fractional Schrödinger equation and light propagation in honeycomb lattice, *Ann. Phys. (Berlin)* 529(9), 1700149 (2017)
89. Q. E. Hoq, P. G. Kevrekidis, and A. R. Bishop, Discrete solitons and vortices in anisotropic hexagonal and honeycomb lattices, *J. Opt.* 18(2), 024008 (2016)
90. L. H. Haddad, C. M. Weaver, and L. D. Carr, The nonlinear Dirac equation in Bose–Einstein condensates (I): Relativistic solitons in armchair nanoribbon optical lattices, *New J. Phys.* 17(6), 063033 (2015)
91. V. E. Vekslerchik, Solitons of a vector model on the honeycomb lattice, *J. Phys. A Math. Theor.* 49(45), 455202 (2016)
92. R. Zhong, N. Huang, H. Li, H. He, J. Lü, C. Huang, and Z. P. Chen, Matter-wave solitons supported by quadrupole quadrupole interactions and anisotropic discrete lattices, *Int. J. Mod. Phys. B* 32(09), 1850107 (2018)
93. Q. Wang and Z. Deng, Multi-pole solitons in nonlocal nonlinear media with fourth-order diffraction, *Results in Physics* 17, 103056 (2020)
94. H. Wang, X. Ren, J. Huang, and Y. Weng, Evolution of vortex and quadrupole solitons in the complex potentials with saturable nonlinearity, *J. Opt.* 20(12), 125504 (2018)
95. G. Chen, Y. Liu, and H. Wang, Mixed-mode solitons in quadrupolar BECs with spin–orbit coupling, *Commun. Nonlinear Sci. Numer. Simul.* 48, 318 (2017)
96. Y. V. Kartashov and D. A. Zezyulin, Stable multiring and rotating solitons in two-dimensional spin–orbit-coupled, Bose–Einstein condensates with a radially periodic potential, *Phys. Rev. Lett.* 122(12), 123201 (2019)
97. C. J. Pethick and H. Smith, Bose–Einstein Condensation in Dilute Gases, New York: Cambridge University Press, 2002
98. L. M. Chiofalo, S. Succi, and P. M. Tosi, Ground state of trapped interacting Bose–Einstein condensates by an explicit imaginary time algorithm, *Phys. Rev. E* 62(5), 7438 (2000)
99. J. Yang and T. I. Lakoba, Accelerated imaginary-time evolution methods for the computation of solitary waves, *Stud. Appl. Math.* 120, 265 (2008)
100. I. M. Merhasin, B. V. Gisin, R. Driben, and B. A. Malomed, Finite-band solitons in the Kronig–Penney model with the cubic–quintic nonlinearity, *Phys. Rev. E* 71, 016613 (2005)
101. R. Driben, B. A. Malomed, A. Gubeskys, and J. Zyss, Cubic–quintic solitons in the checkerboard potential, *Phys. Rev. E* 76, 066604 (2007)